Journal of Sound and Vibration (1999) **219**(4), 559–579
Article No. jsvi.1998.1925, available online at http://www.idealibrary.com.on IDEAL

IMPROVEMENT OF CORNER SHIELDING BY AN ABSORBING CYLINDER

F. P. MECHEL
D-71120 *Grafenau* 1, *Germany*

(*Received* 19 *May* 1998)

This paper continues the topic of the preceding papers [1–3] about sound fields in wedge-shaped spaces, especially of reference [3] which deals with the scattering of sound by building corners. A cylinder surrounding the corner is used there as an analytical instrument to avoid singularities of the field formulation in the origin (the cylinder radius there finally was set to zero). In the present paper the sound field formulation of reference [3] is repeated, with the aim being to study the potential of an absorbing cylinder which surrounds a scattering corner to improve the sound shielding by the corner. The improvement of the corner shielding can be rather high, if a suitable surface admittance can be given to the cylinder. The question of the realization of a suitable cylinder surface admittance is discussed.

1. INTRODUCTION

The present paper is a member of a series of previous papers [1–3], which all have as their common topic sound field analysis in wedge-shaped spaces. The common aim is the field synthesis with wedge modes, which are mutually orthogonal between the wedge flanks. The last contribution [3], deals with sound scattering at rigid corners. In the analysis a hypothetical cylinder is used surrounding the corner in order to avoid the singularities of wedge modes at the origin. There the cylinder was finally eliminated by letting its radius go to zero. The sound field could be split into two parts, one part containing the corner without the cylinder, and a second part representing the contribution to the sound field by the cylinder. This field representation, which will shortly be repeated below, is the basis for the present study, in which the possible contribution of an absorbing cylinder around a corner to the sound shielding by the corner (corner shielding) is investigated.

A typical arrangement is illustrated in Figure 1. A corner with rigid flanks results in a wedge-shaped field space with a wedge angle Θ_0 (e.g., $\Theta_0 = 270^\circ$ in the figure). The corner is surrounded with a cylinder of radius a which is supposed to be locally absorbing with a surface admittance G. Two types are considered for the incident sound. In the first case it is produced by a line source (parallel to the corner) at Q with the coordinates (r_q, ϑ_q). Then two zones of the sound field must be distinguished: zone (1) with $0 \leqslant r \leqslant r_q$, and zone (2) with $r \geqslant r_q$. The second case with an incident plane wave is obtained by letting $r_q \to \infty$; then all the field belongs

0022–460X/99/040559 + 21 $30.00/0

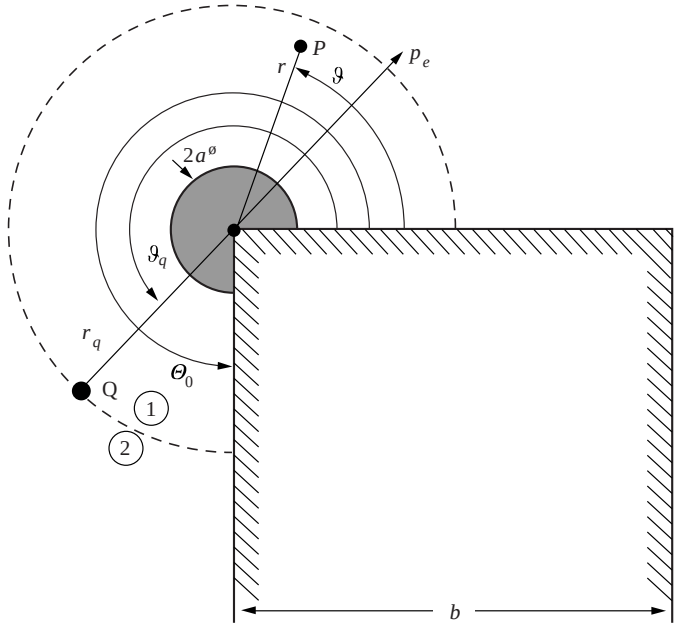

Figure 1. Scheme and coordinates of a rigid corner with "wedge angle" Θ_0 and a line source at Q with coordinates (r_q, ϑ_q). The corner is surrounded by a locally absorbing cylinder with radius a. The source radius r_q defines two field zones (1) and (2).

to zone (1). (Note that in subsequent figures, the coordinates (r, ϑ) in Figure 1 are sometimes expressed in their Cartesian forms $x = r \cos \vartheta$ and $y = r \sin \vartheta$.)

Any wedge angle $0 < \Theta_0 \leqslant 2\pi$ is possible. Thus the theory covers some special cases, as indicated in Figure 2, which individually are of some interest in applications. The first sketch in Figure 2 with $\Theta_0 = 180^\circ$ corresponds to a semicircular absorbing dam on a rigid ground. This case was described in reference [4] where it was compared with dams of semielliptic cross sections. The last sketch in Figure 2 with $\Theta_0 = 360^\circ$ represents a thin rigid screen with an absorbing cylinder atop. This topic was treated by Möser [5], and at the same time by the author [6]. So the present paper is concentrated on arrangements of the second sketch in Figure 2: corners of buildings equipped with an absorbing cylinder. One can imagine situations where this problem is of some practical importance. Many houses in cities are oriented with the windows of living and sleeping rooms towards inner courtyards; such courtyards are often conceived in modern residential quarters as rest areas, protected from the traffic noise by the noise shielding of the building. A similar situation exists with a penthouse on the roof of a building. There the noise shielding is performed by only one building corner. Usually the attitude of acousticians is to take the noise level behind the building corner as it is, as if there were no possibility of noise control engineering in the case of building corners.

First the sound field formulation from reference [3] is repeated. Then some general guidelines will be presented for the design of appropriate absorbing cylinders. Finally numerical examples will be given for the noise level change $\Delta L(r, \vartheta)$ produced by an absorbing cylinder in a field point r, ϑ. This noise level

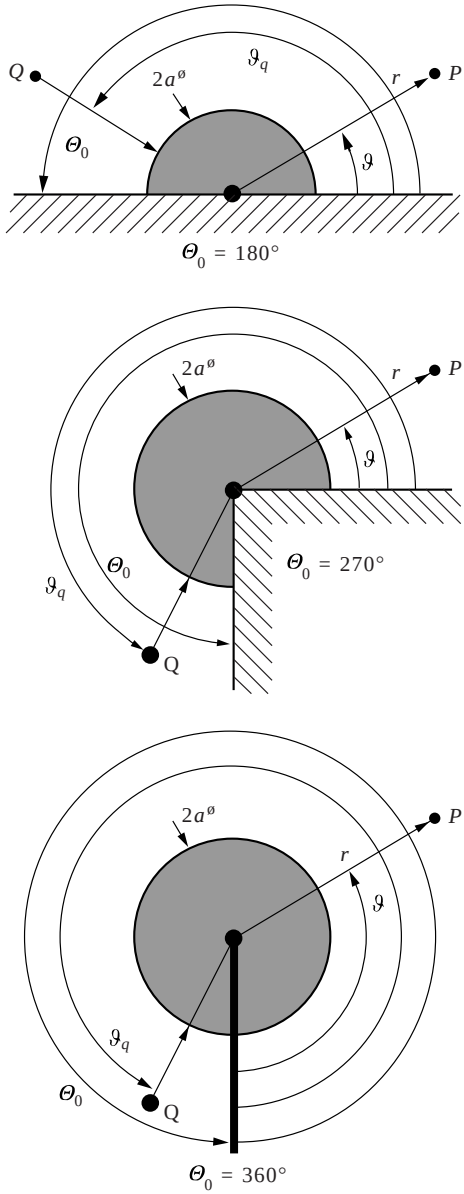

Figure 2. The range of application of the theory covers a semicircular absorbing dam on a rigid ground, a rigid building corner surrounded by an absorbing cylinder, and a rigid, thin screen with an absorbing cylinder atop.

change ΔL can be added to the noise level $L(r, \vartheta)$ in r, ϑ which would exist there if there were no cylinder at the corner (see reference [3] for the computation of $L(r, \vartheta)$).

2. SINGLE CORNER SCATTERING WITH A LINE SOURCE

The coordinates are as shown in Figure 1, with $b \to \infty$ a line source at Q with the source coordinates (r_q, ϑ_q). The source radius r_q defines the zone (1) with

$0 \leqslant r \leqslant r_q$ and the zone (2) with $r \geqslant r_q$. Evidently the sound field must be steady at $r = r_q$, except at $\vartheta = \vartheta_q$. The cylinder with diameter $2a$ at the corner is supposed to have a locally reacting surface with a radial surface admittance G (a rigid cylinder with $G = 0$ is just a special case).

Field formulations are of the form

$$p(r, \vartheta, z) = \sum_{\eta} R_\eta(r) T(\eta\vartheta) Z(k_z z), \tag{1}$$

where the factor $Z(k_z z)$ may be one of the functions $e^{\pm jk_z z}$, $\cos(k_z z)$, $\sin(k_z z)$ or a linear combination thereof with a given wave number k_z. Because $Z(k_z z)$ will appear as a factor in all field representations, one can drop it (like the time factor $e^{j\omega t}$); the only consequence of a value $k_z \neq 0$ will be a modification of the radial wave number $k_0^2 \to k^2 = k_0^2 - k_z^2$. For the numerical examples below it will be supposed that for $k_z = 0$, $Z(k_z z) = 1$, for reasons of simplicity. With two rigid flanks the azimuthal function has the form $T(\eta\vartheta) = \cos(\eta\vartheta)$. The terms under the sum of equation (1) are orthogonal over ϑ in $0 \leqslant \vartheta \leqslant \Theta_0$, and they satisfy the boundary conditions at the flanks if they are solutions of the characteristic equation

$$(\eta_n \Theta_0) \tan(\eta_n \Theta_0) = 0. \tag{2}$$

Solutions of equation (2) are $\eta_n = n\pi/\Theta_0$; $n = 0, 1, 2, \ldots$. The wave equation gives for the radial function $R_\eta(r)$ the Bessel differential equation

$$\left(\frac{\partial^2}{\partial r^2} + \frac{1}{r}\frac{\partial}{\partial r} + k^2 - \frac{\eta_n^2}{r^2}\right) R_{\eta_n}(r) = 0, \tag{3}$$

with general solutions of the form

$$R_\eta(r) = R_n(kr) = c_n \mathrm{H}^{(1)}_{\eta_n}(kr) + d_n \mathrm{H}^{(2)}_{\eta_n}(kr), \tag{4}$$

where $\mathrm{H}^{(i)}_{\eta_n}(kr)$ are Hankel functions, propagating radially inward for $i = 1$ and outward for $i = 2$. They have the orders $\eta_n \geqslant 0$ which either are rational or real in general (depending on the value of Θ_0).

Sound field formulations in zone (1), with $a \leqslant r < r_q$ are

$$p_1(r, \vartheta) = \sum_{n \geqslant 0} A_n \mathrm{H}^{(2)}_{\eta_n}(kr_q)[\mathrm{H}^{(1)}_{\eta_n}(kr) + r_n \mathrm{H}^{(2)}_{\eta_n}(kr)] \cos(\eta_n \vartheta),$$

$$Z_0 v_{r1} = \frac{jk}{k_0} \sum_{n \geqslant 0} A_n \mathrm{H}^{(2)}_{\eta_n}(kr_q)[\mathrm{H}'^{(1)}_{\eta_n}(kr) + r_n \mathrm{H}'^{(2)}_{\eta_n}(kr)] \cos(\eta_n \vartheta), \tag{5}$$

and in the zone (2), with $r_q < r < \infty$ they are

$$p_2(r, \vartheta) = \sum_{n \geqslant 0} A_n [\mathrm{H}^{(1)}_{\eta_n}(kr_q) + r_n \mathrm{H}^{(2)}_{\eta_n}(kr_q)] \mathrm{H}^{(2)}_{\eta_n}(kr) \cos(\eta_n \vartheta),$$

$$Z_0 v_{r2} = \frac{\mathrm{j}k}{k_0} \sum_{n \geqslant 0} A_n [\mathrm{H}^{(1)}_{\eta_n}(kr_q) + r_n \mathrm{H}^{(2)}_{\eta_n}(kr_q)] \mathrm{H}'^{(2)}_{\eta_n}(kr) \cos(\eta_n \vartheta). \tag{6}$$

A prime indicates the derivative with respect to the argument. This formulation satisfies the boundary conditions at the flanks and Sommerfeld's far field condition; it is steady in the sound pressure at the zone limit $r = r_q$. It contains inward and outward propagating modes for $r < r_q$ and only outward propagating modes in $r > r_q$. The factors r_n evidently are radial reflection factors defined at the surface of the cylinder covering the origin. Due to the orthogonality of the modes, the boundary condition at the cylinder must be obeyed term-wise, giving

$$r_n = -\frac{Z_0 G \mathrm{H}^{(1)}_{\eta_n}(ka) + \mathrm{j}\dfrac{k}{k_0} \mathrm{H}'^{(1)}_{\eta_n}(ka)}{Z_0 G \mathrm{H}^{(2)}_{\eta_n}(ka) + \mathrm{j}\dfrac{k}{k_0} \mathrm{H}'^{(2)}_{\eta_n}(ka)}. \tag{7}$$

The still available boundary condition is the fitting of the radial particle velocities at the zone limit $r = r_q$ to the volume flow of the line source: i.e., the relation

$$v_{r2}(r_q + 0) - v_{r1}(r_q - 0) \overset{!}{=} q\, \delta(\vartheta - \vartheta_q), \tag{8}$$

where q is the volume flow density of the source and δ the Dirac delta function. The volume flow density q of the source can be expressed by the free field sound pressure $p_Q(\rho)$ at a distance ρ as

$$Z_0 q = \frac{4}{k_0 \rho \mathrm{H}^{(2)}_0(k\rho)} p_Q(\rho). \tag{9}$$

The expansion of the Dirac function in wedge modes of the form

$$\delta(\vartheta - \vartheta_q) = \sum_{n \geqslant 0} b_n \cos(\eta_n \vartheta), \tag{10}$$

with application of the orthogonality of the modes with the norms N_n,

$$N_n = \frac{1}{\Theta_0} \int_0^{\Theta_0} \cos^2(\eta_n \vartheta)\, \mathrm{d}\vartheta = \frac{1}{2}\left(1 + \frac{\sin(2\eta_n \Theta_0)}{2\eta_n \Theta_0}\right) = \begin{cases} 1, & n = 0 \\ 1/2, & n > 0 \end{cases}, \tag{11}$$

results in

$$\delta(\vartheta - \vartheta_q) = \frac{1}{\Theta_0} \sum_{n \geqslant 0} \frac{1}{N_n} \cos(\eta_n \vartheta_q) \cos(\eta_n \vartheta). \tag{12}$$

The boundary condition (8) must be satisfied term-wise (again because of the orthogonality of the modes), which leads to

$$A_n[\mathrm{H}^{(1)}_{\eta_n}(kr_q)\mathrm{H}'^{(2)}_{\eta_n}(kr_q) - \mathrm{H}'^{(1)}_{\eta_n}(kr_q)\mathrm{H}^{(2)}_{\eta_n}(kr_q)] = -\mathrm{j}\,\frac{k_0}{k}\,\frac{Z_0 q}{\Theta_0 N_n}\cos(\eta_n \vartheta_q). \tag{13}$$

The bracket contains the Wronski determinant of the Hankel functions with the value $[\cdots] = -4\mathrm{j}/(\pi k r_q)$, so one obtains

$$A_n = \frac{\pi}{4}\,k_0 r_q\,\frac{Z_0 q}{\Theta_0 N_n}\cos(\eta_n \vartheta_q) = \frac{\pi}{\Theta_0 N_n}\,\frac{p_Q(0)}{\mathrm{H}^{(2)}_0(kr_q)}\cos(\eta_n \vartheta_q). \tag{14}$$

In the last expression equation (9) has been used, and the free field sound pressure of the source at the corner is denoted by $p_Q(0)$ because the corner is the origin of the coordinate system (r, ϑ).

For a separation of the corner and the cylinder contributions to the field one applies the identity

$$r_n = 1 + (r_n - 1) = 1 - 2C_n, \qquad 2C_n = 1 - r_n, \tag{15}$$

to obtain

$$C_n = \frac{Z_0 G\mathrm{J}_{\eta_n}(ka) + \mathrm{j}\,\dfrac{k}{k_0}\,\mathrm{J}'_{\eta_n}(ka)}{Z_0 G\mathrm{H}^{(2)}_{\eta_n}(ka) + \mathrm{j}\,\dfrac{k}{k_0}\,\mathrm{H}'^{(2)}_{\eta_n}(ka)},$$

$$C_n \xrightarrow[Z_0 G \to 0]{} \frac{\mathrm{J}'_{\eta_n}(ka)}{\mathrm{H}'^{(2)}_{\eta_n}(ka)}, \qquad C_n \xrightarrow[Z_0 G \to \infty]{} \frac{\mathrm{J}_{\eta_n}(ka)}{\mathrm{H}^{(2)}_{\eta_n}(ka)}, \qquad C_n \xrightarrow[ka \to 0]{} 0. \tag{16}$$

With this replacement the field formulations for a corner with a cylinder around the origin become

$$p_1(r, \vartheta) = p_{1,\mathrm{Corner}} + p_{1,\mathrm{Cyl}}$$

$$= \frac{2\pi}{\Theta_0}\,\frac{p_Q(0)}{\mathrm{H}^{(2)}_0(kr_q)} \sum_{n \geqslant 0} \frac{\cos(\eta_n \vartheta_q)}{N_n}\,\mathrm{H}^{(2)}_{\eta_n}(kr_q)\mathrm{J}_{\eta_n}(kr)\cos(\eta_n \vartheta)$$

$$- \frac{2\pi}{\Theta_0}\,\frac{p_Q(0)}{\mathrm{H}^{(2)}_0(kr_q)} \sum_{n \geqslant 0} C_n\,\frac{\cos(\eta_n \vartheta_q)}{N_n}\,\mathrm{H}^{(2)}_{\eta_n}(kr_q)\mathrm{H}^{(2)}_{\eta_n}(kr)\cos(\eta_n \vartheta), \tag{17a}$$

$$p_2(r, \vartheta) = p_{2\mathrm{Corner}} + p_{2\mathrm{Cyl}}$$

$$= \frac{2\pi}{\Theta_0}\,\frac{p_Q(0)}{\mathrm{H}^{(2)}_0(kr_q)} \sum_{n \geqslant 0} \frac{\cos(\eta_n \vartheta_q)}{N_n}\,\mathrm{J}_{\eta_n}(kr_q)\mathrm{H}^{(2)}_{\eta_n}(kr)\cos(\eta_n \vartheta)$$

$$- \frac{2\pi}{\Theta_0}\,\frac{p_Q(0)}{\mathrm{H}^{(2)}_0(kr_q)} \sum_{n \geqslant 0} C_n\,\frac{\cos(\eta_n \vartheta_q)}{N_n}\,\mathrm{H}^{(2)}_{\eta_n}(kr_q)\mathrm{H}^{(2)}_{\eta_n}(kr)\cos(\eta_n \vartheta). \tag{17b}$$

The sound fields in the two zones are thus split into two sums. The first sum does not contain any information about the cylinder, and for $a \to 0$ with the consequence $C_n \to 0$ it becomes the field formulation without the cylinder. The second sum represents the field contribution due to the existence of the cylinder.

One can define a level difference $\Delta L(r, \vartheta)$ at a field point due to the existence of the cylinder:

$$\begin{aligned} \Delta L_i(r, \vartheta) &= 20 \lg |p_{i,\text{Corner}} + p_{i,\text{Cyl}}| - 20 \lg |p_{i,\text{Corner}}| \\ &= 20 \lg |1 + p_{i,\text{Cyl}}/p_{i,\text{Corner}}|, \qquad i = 1, 2. \end{aligned} \tag{18}$$

This is the quantity which will be studied further. It should be noticed that it is reciprocal with respect to the exchange $r, \vartheta \leftrightarrow r_q, \vartheta_q$, because this exchange induces also the exchange of the equations (17a)↔(17b).

3. SINGLE CORNER SCATTERING WITH AN INCIDENT PLANE WAVE

Plane wave incidence is obtained by displacing the line source to infinity, $r_q \to \infty$, letting $\vartheta_q = \text{const}$ and increasing the volume flow density q of the source so that the free field sound pressure $p_Q(0)$ at the corner remains the same. Using the asymptotic expansion of Hankel functions one obtains

$$\frac{\mathrm{H}^{(2)}_{\eta_n}(kr_q)}{\mathrm{H}^{(2)}_{0}(kr_q)} \xrightarrow[r_q \to \infty]{} \mathrm{e}^{\mathrm{j}\eta_n \pi/2} \tag{19}$$

and with this, from equation (17a) (now all the field is in zone (1))

$$\begin{aligned} p(r, \vartheta) &= p_{\text{Corner}} + p_{\text{Cyl}} \\ &= \frac{2\pi}{\Theta_0} p_Q(0) \sum_{n \geqslant 0} \frac{\mathrm{e}^{\mathrm{j}\eta_n \pi/2}}{N_n} \mathrm{J}_{\eta_n}(kr) \cos(\eta_n \vartheta_q) \cos(\eta_n \vartheta) \\ &\quad - \frac{2\pi}{\Theta_0} p_Q(0) \sum_{n \geqslant 0} C_n \frac{\mathrm{e}^{\mathrm{j}\eta_n \pi/2}}{N_n} \mathrm{H}^{(2)}_{\eta_n}(kr) \cos(\eta_n \vartheta_q) \cos(\eta_n \vartheta). \end{aligned} \tag{20}$$

The sound pressure level difference $\Delta L(r, \vartheta)$ due to the cylinder is again given by equation (18).

4. SOME GUIDELINES FOR THE REALIZATION

In this section some guidelines for the improvement of corner shielding by absorbing cylinders shall be derived from numerical examples. The numerical evaluations shall be restricted to a wedge angle $\Theta_0 = 270^\circ$ (i.e., a right-angled corner) and mostly to an incident plane wave. Sound incidence is supposed to be normal to the corner line (i.e., $k_z = 0, k = k_0$). The preference given to plane wave excitation with normal incidence is made because of simplicity in the numerical evaluation. Numerical problems with an excitation by a line source have been discussed in reference [3]. They were obtained with only a limited precision in the

computation of Bessel and Neumann functions. In the present evaluations a more precise—and nevertheless computationally fast—method is applied for the generation of these functions, based on the known recursions

$$J_{\nu-1}(z) = (2\nu/z)J_\nu(z) - J_{\nu+1}(z), \qquad Y_{\nu+1}(z) = (2\nu/z)Y_\nu(z) - Y_{\nu-1}(z).$$

When used in the indicated directions, they are known to "heal" numerical errors of the two initial functions and of the iteration process. If the orders η_n are simple rationals, e.g., $\eta_n = n\pi/\Theta_0 = 2n/3$, $n = 0, 1, 2, \ldots$, for right-angled corners, the functions are evaluated for three sets of orders: $m + 0$, $m + 2/3$, $m + 4/3$, $m = 0, 2, 4, \ldots$, and the wanted set for η_n is composed of these after iteration over $m = 0, 1, 2, \ldots$ (or in the reverse direction). The iterations begin with two start functions which are evaluated with high precision (about 17 digits); the final functions have at least a 15 digit precision. The higher precision is needed here because the argument kr may assume values as high as $kr \approx 200$.

Figure 3(a) shows the field of the sound pressure level $20 \lg |p(r, \vartheta)/p_Q(0)|$ around a corner with a cylinder of a normalized surface admittance $Z_0G = 1 + 0{\cdot}5\mathrm{j}$ and with a fixed $ka = 2{\cdot}5$. Sound incidence of a plane wave with $\vartheta_q = 270^\circ$ is parallel to one corner flank. In Figure 3(b) the angle of sound incidence is reduced to $\vartheta_q = 225^\circ$. Whereas the sound field on the illuminated side is relatively simple in Figure 3(a) (small standing wave oscillations from the superposition of the incident plane wave and a cylindrical scattered wave), it becomes rather complex in Figure 3(b): a strong standing wave pattern of a plane wave on front of a rigid wall, disturbed by an additional cylindrical scattered wave from the corner. The sound field in the shadow area is simple in both cases: a steep decrease towards the second flank. The sound pressure level increase in the immediate neighbourhood of the flank indicates a wave which is directed towards the flank and rigidly reflected there. This is different from the pattern with no cylinder (see reference [3]); there the field level in the shadow zone approaches the flank with a horizontal slope in the azimuthal direction over larger distances from the flank as would be produced by an omnidirectional line source in the corner. The shadow with the cylinder is deeper than for a corner without the cylinder. The sound pressure near to the flank levels off with increasing radial distance kr.

Next, Figure 4(a) shows the sound pressure level difference $\Delta L(r, \vartheta)$ due to the cylinder for a plane wave parallel to the illuminated flank, $\vartheta_q = 270^\circ$; the cylinder is characterized by $ka = 2{\cdot}5$ and $Z_0G = 1 - 0{\cdot}5\mathrm{j}$. The sound pressure level is reduced by the cylinder by about $\Delta L \approx -30$ dB immediately at the cylinder and still by about $\Delta L \approx -10$ dB at larger distances near to the flank. It is interesting to notice that the level reduction begins already on the illuminated side: i.e., at $\vartheta > 90^\circ$. In Figure 4(b) only the angle of sound incidence is changed to $\vartheta_q = 225^\circ$. $\Delta L(r, \vartheta)$ on the illuminated side now has strong narrow peaks at places, where the sound field without the cylinder has deep interference minima; therefore the high peaks of $\Delta L(r, \vartheta)$ there have no practical importance. The level difference $\Delta L(r, \vartheta)$ in the shadow zone has a similar shape as in Figure 4(a); however the level reduction now is not as strong as there. Figure 4(c) with $\vartheta_q = 180^\circ$, i.e., with the sound wave incident parallel to the second flank, is remarkable insofar as it shows that some level reduction is produced by the cylinder even in that limit case.

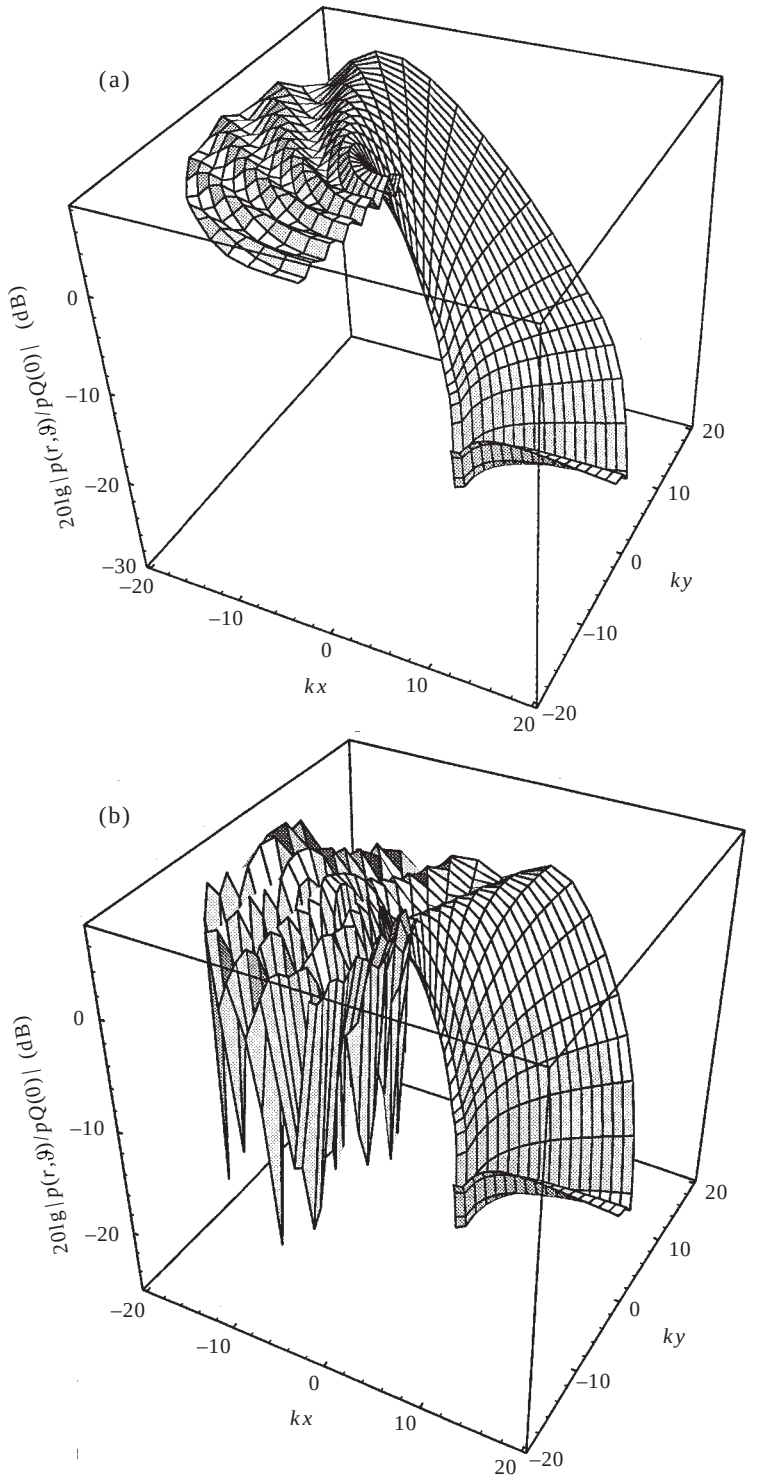

Figure 3. (a) Sound pressure level around a right-angled corner with an absorbing cylinder, excited by a plane wave incident parallel to one flank, $\vartheta_q = \Theta_0 = 270°$; (b) as (a) but for $\vartheta_q = 225°$, $ka = 2{\cdot}5$, $Z_0G = 1 + 0{\cdot}5\mathrm{j}$.

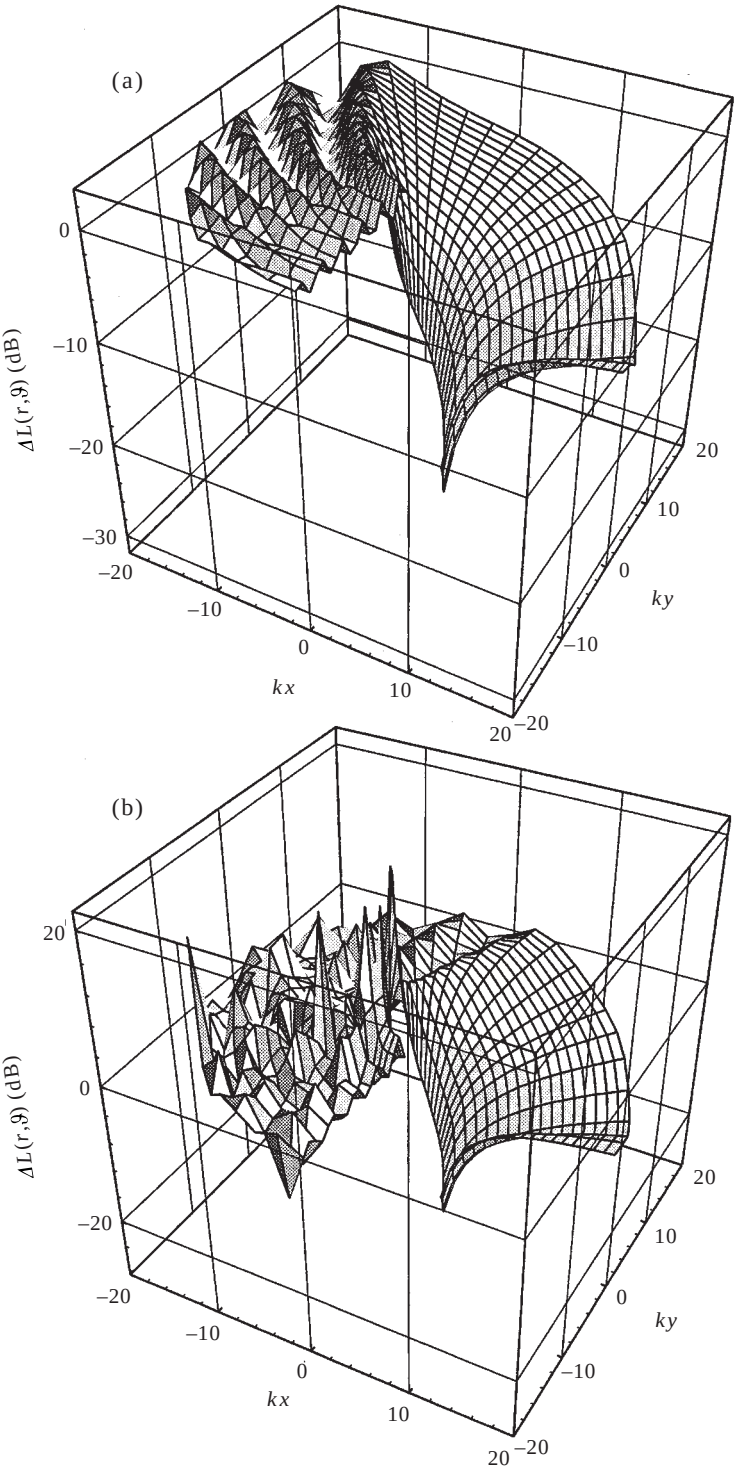

Figure 4—(*Caption on opposite page*).

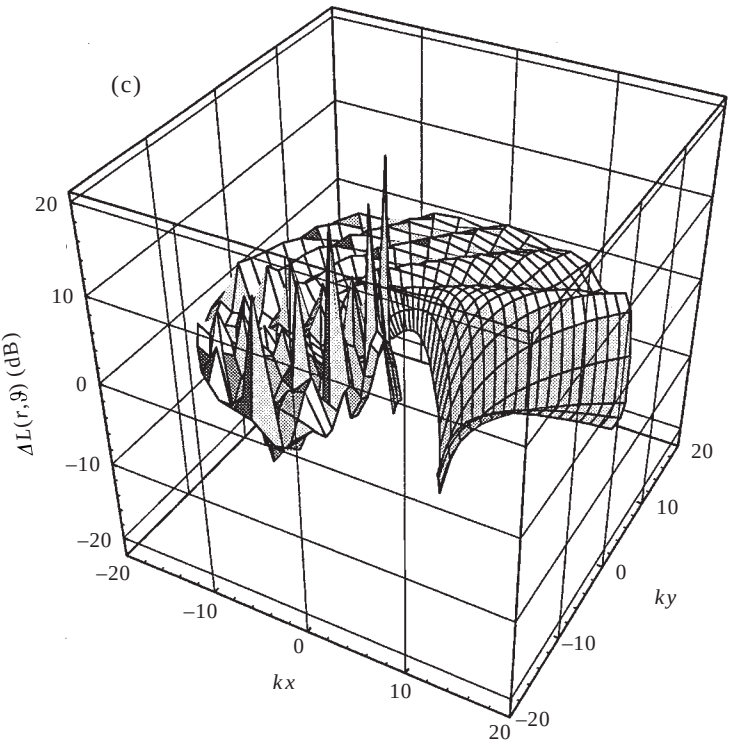

Figure 4. (a) Sound pressure level difference $\Delta L(r, \vartheta)$ around a right-angled corner produced by an absorbing cylinder, excited by a plane wave incident parallel to one flank, $\vartheta_q = \Theta_0 = 270°$; (b) as (a) but for $\vartheta_q = 225°$; note that peaks on the illuminated side are at places where the sound field without the absorbing cylinder has deep standing wave minima; (c) as (b) but for $\vartheta_q = 180°$: i.e., gracing incidence on the second flank. $ka = 2{\cdot}5$, $Z_0G = 1 - 0{\cdot}5$j.

For the demonstration of the influence which some parameters have on the sound pressure level difference $\Delta L(r, \vartheta)$ one can take field points on the flank of the shadow side, $\vartheta = 0$. In Figure 5, with a cylinder characterised by $ka = 2{\cdot}5$, $Z_0G = 1 + 1$j, the angle ϑ_q of sound incidence is changed; the efficiency of the cylinder increases with increasing angle source-corner-field point. Figure 6 with $\vartheta_q = 225°$ and $Z_0G = 1 + 1$j shows $\Delta L(r, 0)$ over kr for different values of ka. It is quite plausible that the efficiency of the cylinder increases with ka. However, there is still the question whether there are peculiar values of ka. This aspect is illustrated in Figures 7 and 8, both for a line source. In Figure 7 the source is at a distance $kr_q = 11$ with different source angles ϑ_q; the receiving point is on the second flank, $\vartheta = 0$, at a distance $kr = 20$. The sound pressure level difference $\Delta L(kr, 0)$ is plotted against ka for a cylinder with fixed (normalized) surface admittance $Z_0G = 1 + 1$j. For low ka values the order of the curves with different ϑq can be reversed, but for larger ka values the efficiency of the cylinder increases with the deflection angle source-corner-field point. And special values of ka are not visible. Figure 8, again with $\Delta L(kr, 0)$ against ka, for a line source at $kr_q = 20$, $\vartheta_q = 225°$ and the field point at $kr = 40$, $\vartheta = 0$, shows changes with the value of

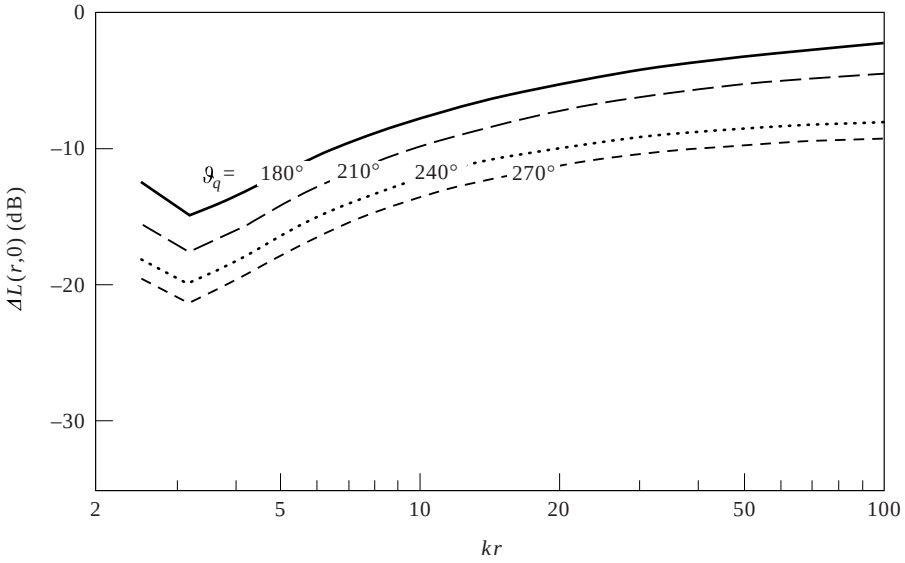

Figure 5. Sound pressure level difference $\Delta L(r, 0)$ produced by the absorbing cylinder along the shadowed flank ($\vartheta = 0$) for plane wave incidence with different source angles ϑ_q; for the cylinder $ka = 2{\cdot}5$ and $Z_0G = 1 + \mathrm{j}$; $\Theta_0 = 270^\circ$.

Z_0G. Both diagrams indicate a rather monotonic increase of the cylinder efficiency with ka and the absence of special ka values.

An important question is: which values of Z_0G are necessary for large level reductions $-\Delta L$? To deduce some guidelines one can take a fixed value of $ka = 5$ (of medium size) and a fixed field point distance $kr = 50$ (not too small) and keep

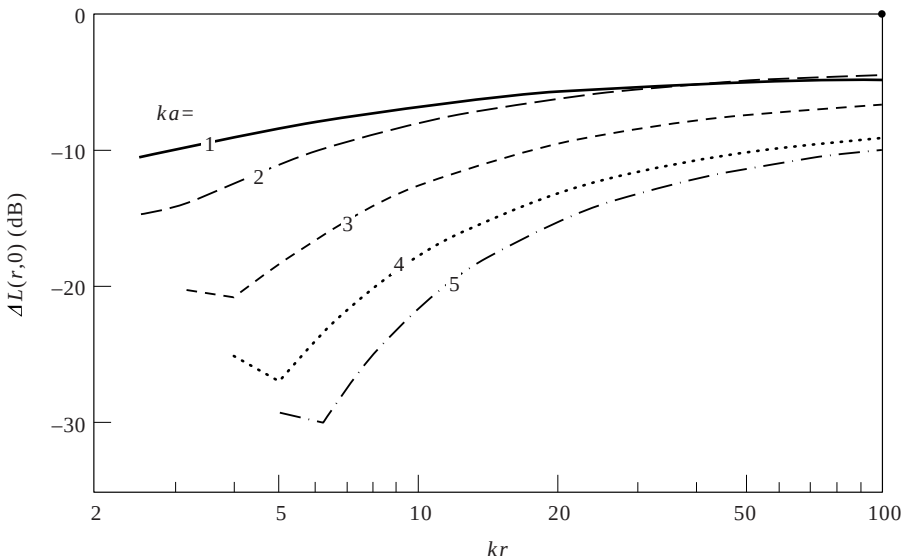

Figure 6. Sound pressure level difference $\Delta L(r, 0)$ produced by the absorbing cylinder for different ka values along the shadowed flank ($\vartheta = 0$) for plane wave incidence with source angle $\vartheta_q = 225^\circ$; cylinder admittance $Z_0G = 1 + \mathrm{j}$; $\Theta_0 = 270^\circ$.

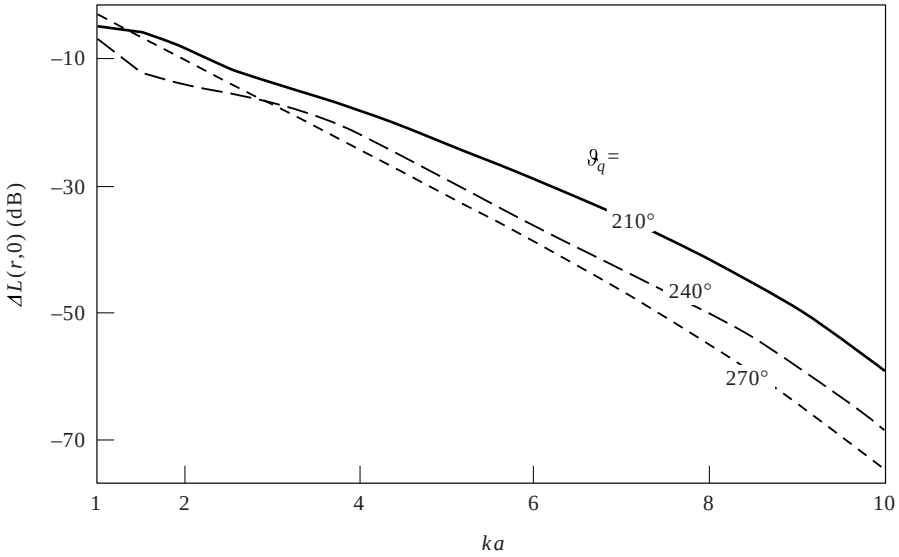

Figure 7. Sound pressure level difference $\Delta L(r, 0)$ produced by the absorbing cylinder at the shadowed flank ($\vartheta = 0, kr_q = 11$) as a function of ka for cylindrical wave incidence with different source angles ϑ_q; cylinder admittance: $Z_0G = 1 + \mathrm{j}$; $\Theta_0 = 270^\circ$, $kr = 20$.

also ϑ_q on a fixed value ($\vartheta_q = 270^\circ = \Theta_0$ in the examples shown). Then one can plot $\Delta L(r, 0)$ over the complex plane of Z_0G. Figure 9(a) is such a 3D-plot (for an incident plane wave). The most pronounced feature of this diagram is the peak of $\Delta L(r, 0)$ at the imaginary axis between about $-1 < \mathrm{Im}\{Z_0G\} < +1$. The maximum is at about $\mathrm{Im}\{Z_0G\} \approx +0{\cdot}5$ but even there positive values are

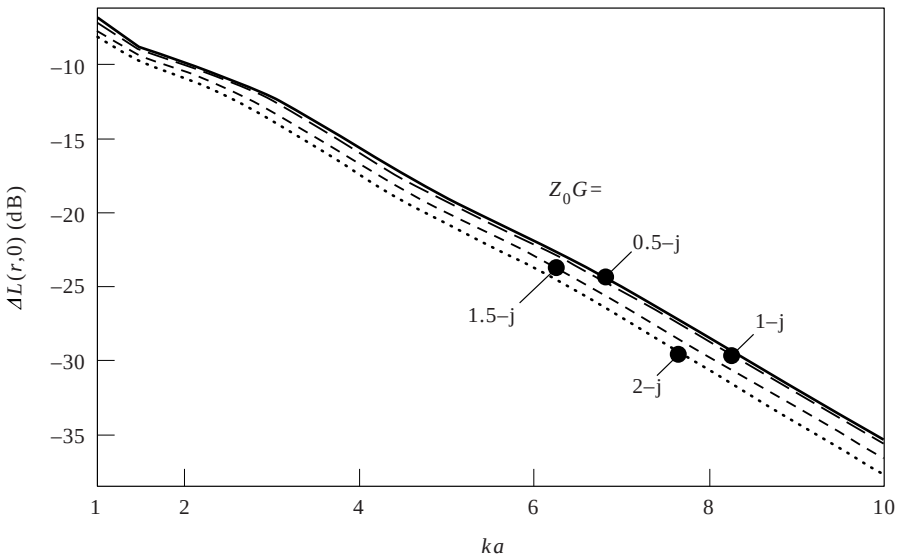

Figure 8. Sound pressure level difference $\Delta L(r, 0)$ produced by the absorbing cylinder at the shadowed flank ($\vartheta = 0, kr = 40$) as a function of ka for cylindrical wave incidence for some values of the cylinder surface admittance Z_0G. $\Theta_0 = 270^\circ$, $\vartheta_q = 225^\circ$, $kr_q = 20$.

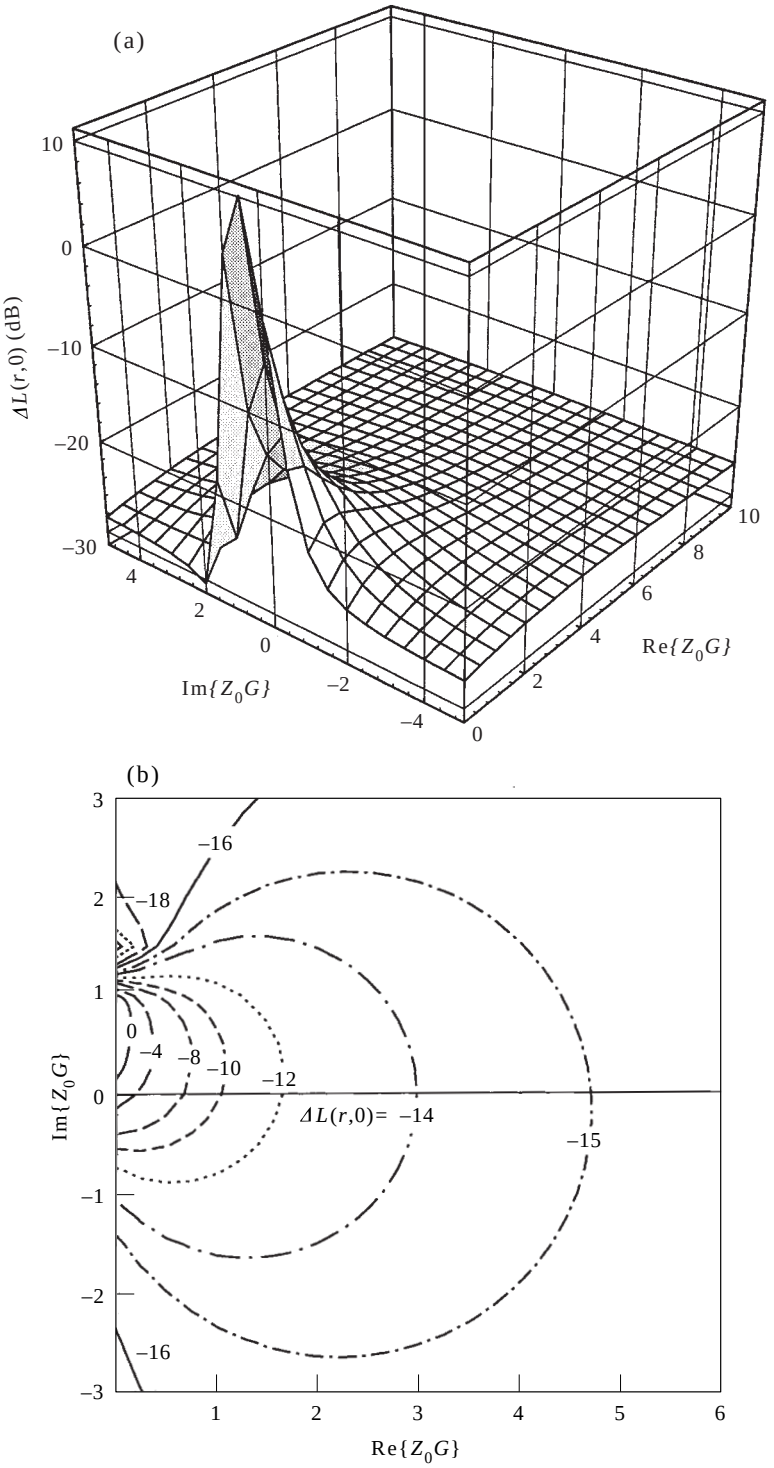

Figure 9. (a) Sound pressure level difference $\Delta L(r, 0)$ produced by the absorbing cylinder at the shadowed flank for $kr = 50$ over the complex plane of the normalized cylinder surface admittance Z_0G; (b) as (a) but represented as a contour plot. $\Theta_0 = 270^\circ$, $\vartheta_q = 270^\circ$, $ka = 5$.

assumed by $\Delta L(r, 0)$: i.e., the cylinder produces higher levels at the field point than the corner without the cylinder. Along the real axis the range of small (or even negative) cylinder efficiency is restricted to about $0 \leqslant \mathrm{Re}\{Z_0 G\} < 0{\cdot}5$. Outside the region of the peak the precise value of $Z_0 G$ is not very important. Note that, the minimum value of $\Delta L(r, 0)$ is obtained "behind" the peak (as seen from the origin), near the positive imaginary axis. The peak of $\Delta L(r, \vartheta)$ near the positive imaginary axis of $Z_0 G$ is produced by surface waves which exist at the cylinder under such conditions; they may "brighten" the shadow behind the cylinder.

The plot of $\Delta L(r, 0)$ over the complex plane of $Z_0 G$ can be made usable as a design tool, if one plots it as a contour diagram. This is done in Figure 9(b) for the special parameter values $\vartheta_q = 225^\circ$, $ka = 5$ and $kr = 50$. One could suggest drawing the curve of $Z_0 G$ of a guessed absorber in this diagram for a running frequency f. In principal that would be a contradiction, because ka, kr are supposed to be constant. However, numerical experiments with many values of ka, kr have shown, that the *pattern* and the *position* of the contour curves remain about unchanged. Thus Figure 9(b) can be used as a *template* for complex curves of $Z_0 G$ if one avoids definite values of $\Delta L(r, 0)$ at the contour lines. Therefore this graph can be used for the discussion of general guidelines in the design of cylinder absorbers.

The absorbers here can be assumed to end with a rigid inner termination; hence the complex curve of $Z_0 G$ will start at sufficiently low frequencies in or near the origin and will tend into the upper quadrant; its further course for increasing frequency will be composed by a sequence of circular arcs. Absorbers with small losses will initially remain with $Z_0 G$ close to the positive imaginary axis: i.e., they will run into the unfavourable peak of $\Delta L(r, 0)$. This can be avoided by two means. One of them is to apply a low-tuned resonator with a high mass reactance; the peak will be traversed at frequencies below the range of interest, and then the curve of $Z_0 G$ will deflect downward to the lower quadrant. However, with this method the mass reactance will become dominant for higher frequencies and the curve then will remain near the origin: i.e., in the range of small magnitude of $\Delta L(r, 0)$. The second method to avoid the peak consists of the application of sufficiently high losses, selected so as to permit values of $\mathrm{Re}\{Z_0 G\} \approx 1$ or higher. If structures of the absorber are used which show multiple resonances, then structures should be avoided which approach the origin at every anti-resonance (like $\lambda/4$ resonators or foil resonators with low losses).

5. EXAMPLES OF REALIZATION

Somewhat independent of the structure of the absorber is the value of ka of the cylinder: i.e., of its radius a for a given frequency range of interest which one can select as $100 \leqslant f \leqslant 2000$ Hz. Then a radius $a = 0{\cdot}5$ m is a reasonable measure. If the absorber contains air or porous absorber layers, its surface admittance should be computed in principle with Bessel functions (see e.g., reference [7]). If the depth of the absorber is only a part of the radius a, then it is sufficient approximation to compute $Z_0 G$ for a plane absorber arrangement (this approximation is applied in the following examples).

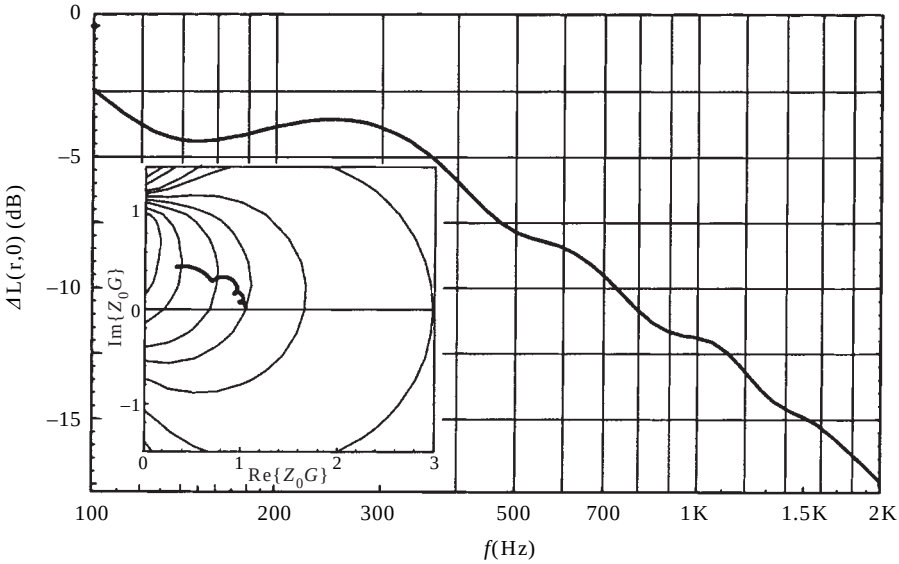

Figure 10. Sound pressure level difference $\Delta L(r, 0)$ due to a cylinder of radius $a = 0{\cdot}5$ m with a locally reacting absorber surface of a glass fiber layer of thickness $t = 0{\cdot}25$ m with flow resistivity $\Xi = 5000$ Pa s/m^2, covered with a perforated sheet of porosity $\sigma = 0{\cdot}45$, 1 mm thick with holes of 5 mm width. The complex curve Z_0G of this absorber is shown in the inset diagram. $\Theta_0 = 270^\circ$, $\vartheta_q = 225^\circ$, $r = 5$ m.

A very simple example for an absorber is a layer of thickness $t < a$ of a porous absorber material which is made locally reacting by radial vanes. The inset in Figure 10 shows Z_0G of a layer of thickness $t = 0{\cdot}25$ m of glass fibre absorber with a flow resistivity $\Xi = 5000$ Pa s/m^2, covered with a perforated metal sheet (at some distance from the porous absorber, as a mechanical protection of the absorber) having a surface porosity of $\sigma = 45\%$, a thickness of 1 mm and holes of 5 mm diameter (the value of Ξ is at the lower end of commercially available glass fibre materials). The curve of Z_0G in its complex plane is shown with the contour lines of Figure 9(b); the frequency steps through 100 Hz $\leqslant f \leqslant$ 2000 Hz with a step of $\Delta \lg(f) = 0{\cdot}025$ (about 1/4 of one-third octave steps). Figure 10 shows $\Delta L(r, 0)$ with $\vartheta_q = 225^\circ$ of the plane wave and the field point at a distance $r = 5$ m on the second flank, i.e., $\vartheta = 0$; ka changes over the range $0{\cdot}9 \leqslant ka \leqslant 18{\cdot}3$ and kr over $9 \leqslant kr \leqslant 183$. When the curve Z_0G with increasing frequency has left the neighbourhood to the peak range, the efficiency $-\Delta L(r, 0)$ continuously increases.

The absorber arrangements of the cylinder in Figure 11 are the same, except a thin, tight, limp foil (which can freely vibrate) behind the perforated sheet now covers the layer of the glass fibre material. Such foils would be favourable as a weather protection. In one case the surface mass density of the foil is $m_f = 0{\cdot}1$ kg/m^2; in the other case $m_f = 0{\cdot}3$ kg/m^2. As can be seen from the Z_0G curves, the mass reactance of the foil brings these curves at higher frequencies too close to the peak range; large positive values of $\Delta L(r, 0)$, i.e., higher levels with the cylinder than without it, are assumed over a wide frequency range with the heavier foil.

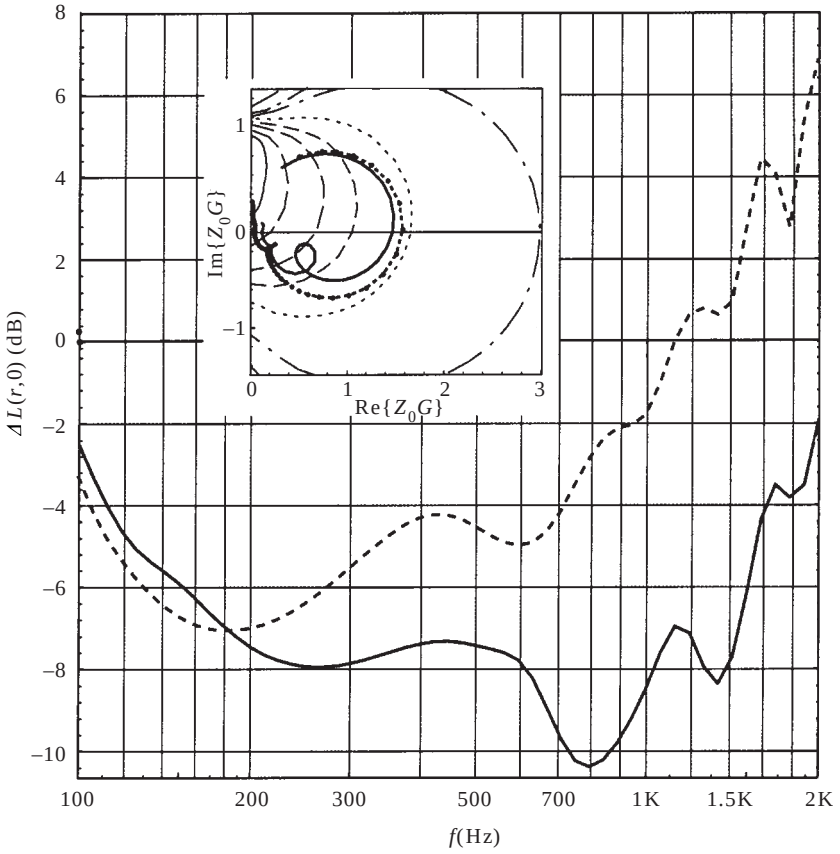

Figure 11. Sound pressure level difference $\Delta L(r, 0)$ due to a cylinder of radius $a = 0{\cdot}5$ m with a locally reacting absorber surface of a glass fiber layer of thickness $t = 0{\cdot}25$ m with flow resistivity $\Xi = 2000$ Pa s/m^2, covered with a perforated sheet of porosity $\sigma = 0{\cdot}45$, 1 mm thick with holes of 5 mm width, and a tight, limp foil between perforated sheet and layer having surface mass densities $m_f = 0{\cdot}1$ kg/m^2 (full line) and $m_f = 0{\cdot}3$ kg/m^2 (dashed line). The complex curves Z_0G of these absorbers are shown in the inset diagram. $\Theta_0 = 270^\circ$, $\vartheta_q = 225^\circ$, $r = 5$ m.

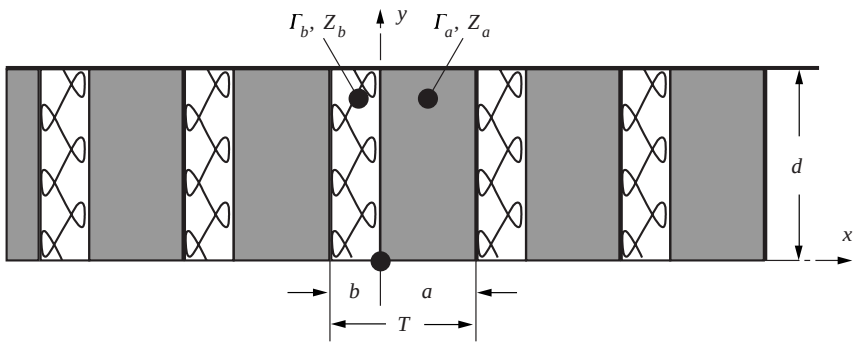

Figure 12. Scheme of a cross-layered absorber. The layers a are porous materials, backed with foils; the layers b are air gaps, possibly with distance holders.

A typical situation with porous sound absorber materials in the present application is that the available flow resistivity values Ξ are too high to permit large Z_0G values. Very low bulk densities cannot be used to reduce Ξ, because the mechanical stability of the material in the (relatively thick) layers would become too low. In such situations the *cross-layered* absorber, see Figure 12, can be brought in. It consists of a sequence of layers a, b oriented normal to the absorber surface, where the layers a (thickness t_a) are commercially available mineral fibre boards (or felts), possibly coated on one side with an aluminium foil (otherwise foils are loosely inserted; they uncouple neighbour elements and make the total arrangement a locally reacting absorber). The layers b (thickness t_b) are air gaps or layers of distance holders like mats of scrambled wire. A couple of layers is treated as a short (length d) silencer duct section the propagation constant (lowest mode) of which can be determined with known methods, from which the average surface admittance of the arrangement can be easily computed (for details see reference [6], chapter 32).

Figures 13(a, b) show the surface admittance Z_0G of cross-layered absorbers and the sound pressure level difference $\Delta L(r, 0)$ obtained with them. The thickness of the absorber is $d = 0{\cdot}15$ m; the layers a are of glass fibre and $t_a = 0{\cdot}05$ m thick; their flow resistivity Ξ gives the normalized flow resistance $\Xi t_a/Z_0 = 1$. The layers b with thickness $t_b = 0{\cdot}02$ m are air gaps. In one modification of the absorber its surface is free (solid lines), in the other modification (dashed line) the surface is covered with a thin, limp foil with a surface mass density $m_f = 0{\cdot}1$ kg/m^2. The absorbers are built in a cylinder with radius $a = 0{\cdot}5$ m, and $\Delta L(r, 0)$ is computed for $\vartheta_q = 240^\circ$ at a field point at $r = 5$ m, $\vartheta = 0$.

The absorber for the last example of Figures 14(a, b) consists of two Helmholtz resonators in series. The resonator volume depths are $t_1 = 0{\cdot}1$ m, $t_2 = 0{\cdot}05$ m; the widths of the resonator volumes at the neck plates in azimuthal direction are 0·1 and 0·08 m, respectively, the resonator plates have slit-shaped openings 0·02 m wide, and the neck lengths are 0·01 m. The losses are produced by flow resistances in the neck orifices (wire meshes) with values $0{\cdot}05Z_0$ and $0{\cdot}15Z_0$, respectively. The curve of Z_0G is composed of two circles (which in Figure 14(a) partially become polygons because of the finite frequency step $\Delta \lg(f) = 0{\cdot}025$). The curve of $\Delta L(r, 0)$ in Figure 14(b) shows strong variations according to the repeated approximation of the Z_0G curve to the peak range.

6. CONCLUSION

The examples shown illustrate that rather broad-banded sound pressure level reductions $-\Delta L$ with magnitudes higher than about 8 dB can be realized with absorbing cylinders at a scattering corner. The reductions can be added to the sound pressure level reductions as produced by the scattering corner alone; these were computed in reference [3]. The improvement produced by a cylinder can be of the order of magnitude of the corner shielding. The noise control engineer indeed has a possibility to reduce the noise level behind an arrangement of buildings.

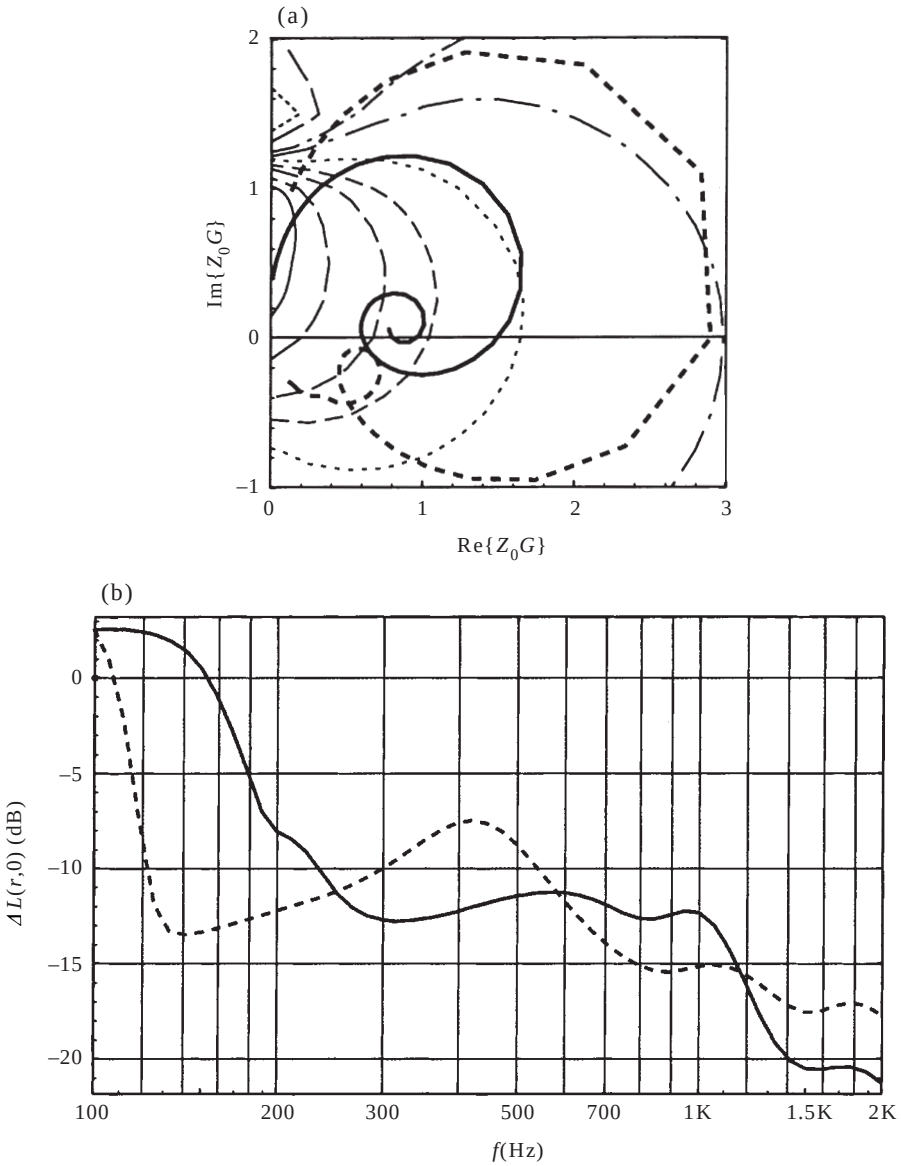

Figure 13. (a) Curves Z_0G in their complex plane of cross-layered absorbers, consisting of glass fibre boards ($t_a = 50$ mm, $\Xi t_a/Z_0 = 1$), covered with a heavy foil on one side, and $t_b = 20$ mm wide air gaps; the absorber with the full line is $d = 0{\cdot}15$ m thick and uncovered, and the absorber with the dashed line is $d = 0{\cdot}25$ m thick and covered with a tight, limp foil of surface mass density $m_f = 0{\cdot}1$ kg/m^2. (b) $\Theta_0 = 270^\circ$, $\vartheta_q = 240^\circ$, $a = 0{\cdot}5$ m, $r = 5$ m. Sound pressure level difference $\Delta L(r, 0)$ produced by a cylinder of radius $a = 0{\cdot}5$ m with the cross-layered absorbers of Figure 13(a).

It is important that the surface admittance Z_0G of the cylinder has high magnitudes and avoids the positive imaginary axis in the range of about $0 \leqslant \mathrm{Re}\,\{Z_0G\} \leqslant 1$. A rigid cylinder of equal size ($Z_0G = 0$) would produce only a marginal level reduction.

Analogous computations for a thin rigid screen ($\Theta_0 = 2\pi$) show that quite similar requirements exist for absorbing cylinders on screens as for cylinders at

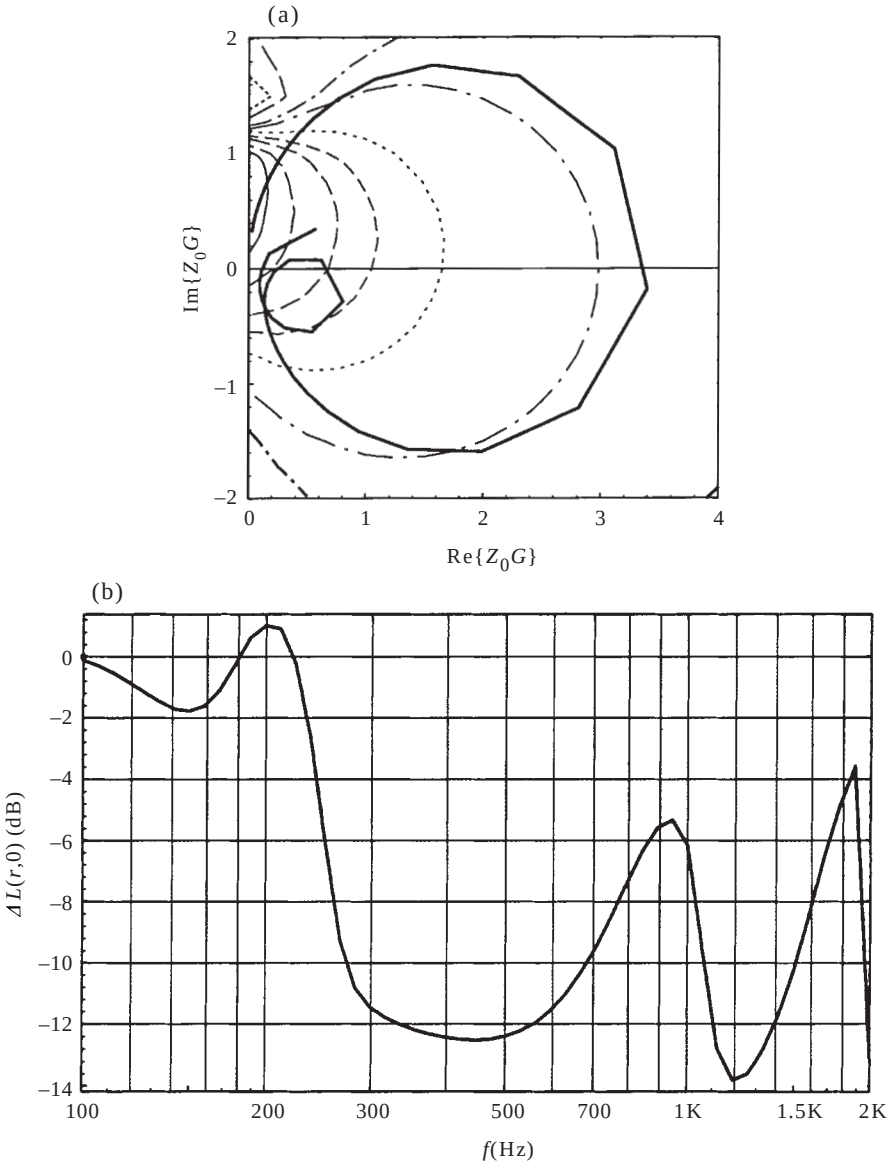

Figure 14. (a) Curve of Z_0G of a double Helmholtz resonator (in series) with volume depths $t_1 = 10$ cm, $t_2 = 5$ cm, volume widths (in azimuthal direction) 10 cm, 8 cm (different according to the conical section into which the resonators are placed), widths of the slit-shaped necks 2 cm, 1 cm, lengths of the necks 1 cm; the orifices are covered with wire mesh of flow resistances $0{\cdot}05Z_0$, $0{\cdot}15Z_0$, respectively. (b) Sound pressure level difference $\Delta L(r, 0)$ produced by a cylinder of radius $a = 0{\cdot}5$ m with the double Helmholtz resonators of Figure 14(a). $\Theta_0 = 270^\circ$, $\vartheta_q = 225^\circ$, $a = 0{\cdot}5$ m, $r = 5$ m.

corners. Therefore the above examples can be used for screens also. Only the resulting values of $\Delta L(r, \vartheta)$ are different—larger absolute magnitudes for screens than for corners.

The effect of an absorbing cylinder at a corner can be qualitatively explained as follows: For a cylinder by itself, a scattered wave would be produced, which in the shadow zone may partially cancel out the incident wave and so determine

the depth of the shadow. For cylinders with deep shadows due to their surface admittance, the scattered wave is of the order of magnitude of the incident wave and of opposite phase. The sound field behind a corner is reduced by the corner scattering. So the cancellation efficiency of the scattered wave of the cylinder can be very high in combination with a corner. It is known that cylinder surfaces with a spring type reactance can guide surface waves (creeping waves) into the shadow zone which leads to "bright" shadows. Under the conditions of surface wave existence the cylinder at the corner will produce higher sound pressure levels in the shadow zone than the corner alone.

REFERENCES

1. F. P. Mechel *Journal of Sound and Vibration* In press. Modes in lined wedge-shaped ducts.
2. F. P. Mechel *Journal of Sound and Vibration* In press. Modal analysis in lined wedge-shaped ducts.
3. F. P. Mechel 1999 *Journal of Sound and Vibration* **219**, 105–132. Scattering at rigid building corners.
4. F. P. Mechel 1997 *Acta Acustica* **83**, 260–283. A uniform theory of sound screens and dams.
5. M. Möser 1995 *Acustica* **81**, 565–586. Die Wirkung von zylindrischen Aufsätzen and Schallschirmen.
6. F. P. Mechel *Schallabsorber*. Stuttgart: Hirzel. See vol. III, chap. 23. Schallschirm mit absorbierendem Zylinder-Aufsatz.
7. F. P. Mechel 1998 *Acta Acustica* **84**, 201–222. Modal solutions in circular and annular ducts with locally or bulk reacting lining.